

What Limits the Efficiency of High-Power InGaN/GaN Lasers?

Joachim Piprek, *Senior Member, IEEE*

Abstract—Blue light emitting InGaN/GaN lasers currently exhibit less than 40% wall-plug efficiency, while infrared InGaAs/GaAs laser diodes exceed 70%. This paper explores the reasons behind the efficiency limitation by the numerical analysis of measured InGaN/GaN laser characteristics. The study reveals a strong increase of the threshold current due to self-heating. The influence of Auger recombination, electron leakage, free-carrier absorption, and series resistance changes with rising injection current.

Index Terms—Semiconductor lasers, numerical analysis.

I. INTRODUCTION

NOBEL laureate Shuji Nakamura predicted in 2014 that GaN-based laser diodes may enable the next generation of solid state lighting (SSL) [1]. The main driving force behind SSL applications is the high energy efficiency of InGaN/GaN light-emitting diodes (LEDs), some of which achieve more than 80% wall-plug efficiency (η_{WPE}) [2]. But the highest η_{WPE} reported for GaN-based laser diodes is still below 40% [3]–[5]. In comparison, some infrared InGaAs/GaAs lasers reach $\eta_{WPE} > 70\%$ at room temperature [6]. We here investigate the reasons for the efficiency limitation of GaN-based lasers by numerical analysis of measured laser characteristics.

The light output power $P(I)$ of a semiconductor laser is typically described as function of the injected current I by

$$P(I) = \frac{h\nu}{q} \eta_i \frac{\alpha_m}{\alpha_m + \alpha_i} (I - I_{th}) \quad (1)$$

with the photon energy $h\nu$, the electron charge q , the differential internal efficiency η_i , the internal absorption loss α_i , and the mirror loss α_m . The threshold current I_{th} compensates for carrier losses. Under ideal conditions without self-heating, these carrier losses do not rise above threshold since the active layer carrier density n_{th} remains constant (clamped).

The wall-plug efficiency is defined as ratio of light output power to electrical input power IV (V - bias)

$$\eta_{WPE}(I) = \frac{h\nu}{qV} \eta_i \eta_{opt} \frac{I - I_{th}}{I} = \eta_{ele} \eta_i \eta_{opt} \eta_{th} \quad (2)$$

including the electrical efficiency $\eta_{ele} = h\nu/qV$, the optical efficiency $\eta_{opt} = \alpha_m/(\alpha_m + \alpha_i)$, and the threshold current efficiency $\eta_{th} = (I - I_{th})/I$. However, this popular analytical

model is somewhat ambiguous when the laser experiences relevant self-heating which typically leads to a sub-linear $P(I)$ characteristic. As the internal laser temperature rises with increasing current, most parameters in above equations change. The photon energy $h\nu(I)$ red-shifts due to band-gap shrinkage, the threshold current $I_{th}(I)$ rises together with the threshold carrier density $n_{th}(I)$ due to declining material gain in the active layers, the differential internal efficiency $\eta_i(I)$ may drop due to increasing carrier leakage, and the optical efficiency $\eta_{opt}(I)$ may suffer from rising internal absorption $\alpha_i(I)$. A previous analytical efficiency study of nitride lasers neglects most of these changes [7]. For a more in-depth efficiency analysis, we here utilize numerical simulations of measured laser characteristics in order to identify the physical processes that limit the wall-plug efficiency of InGaN/GaN lasers.

The simulations are performed using the LASTIP software [8]. The code self-consistently computes carrier transport, the wurtzite electron band structure of strained InGaN quantum wells (QWs), stimulated photon emission, wave guiding, and heat flow. Schrödinger and Poisson equations are solved iteratively in order to account for the QW deformation with changing device bias (quantum-confined Stark effect). The transport model includes drift and diffusion of electrons and holes, Fermi statistics, built-in polarization and thermionic emission at hetero-interfaces. It accounts for all relevant recombination mechanisms, namely Shockley-Read-Hall (SRH) and Auger recombination as well as spontaneous and stimulated photon emission. More details on laser models and material parameters can be found elsewhere [9], [10].

Our experimental reference device is a recently documented 405 nm InGaN/GaN Fabry-Perot laser featuring a record-high light output power of $P=7.2\text{W}$ at $I=4\text{A}$ input current and $V=6.3\text{V}$ bias in continuous-wave (CW) operation at room temperature [5]. The layer structure is given in Table 1. The high output power was mainly accomplished by (a) reducing the thermal resistance to 6.6 K/W [11] and (b) inserting thick undoped GaN waveguide layers that limit the modal overlap with the strongly absorbing p-doped layers [5]. Refractive index profile and lasing mode intensity are plotted in Fig. 1. The p-AlGaIn electron blocking layer (EBL) was moved to the p-side edge of the GaN waveguide in order to minimize the bias [5]. The cavity length is 1.2mm and the ridge width $12\mu\text{m}$. The facet reflectance is 0.056 in the front and 0.95 in the back, resulting in a mirror loss parameter of $\alpha_m = 12/\text{cm}$.

Other crucial parameters are obtained by simulating the published laser performance (Fig. 2) and summarized in Tab. 2. The threshold current is mainly controlled by QW Auger

Manuscript received September 14, 2016; revised December 13, 2016; accepted December 15, 2016. Date of publication December 23, 2016; date of current version January 13, 2017.

J. Piprek is with the NUSOD Institute LLC, Newark, DE 19714-7204 USA (e-mail: piprek@nusod.org).

Color versions of one or more of the figures in this paper are available online at <http://ieeexplore.ieee.org>.

Digital Object Identifier 10.1109/JQE.2016.2644861

TABLE I
EPITAXIAL LASER STRUCTURE [5]

Layer	Composition	Thickness
p-cladding	Al _{0.026} GaN:Mg	660 nm
p-EBL	Al _{0.36} GaN:Mg	5 nm
waveguide	GaN	250 nm
waveguide	In _{0.008} GaN	100 nm
quantum well	In _{0.066} GaN	7.5nm
barrier	In _{0.008} GaN	20 nm
quantum well	In _{0.066} GaN	7.5 nm
waveguide	In _{0.008} GaN	40 nm
waveguide	GaN	450 nm
n-cladding	Al _{0.026} GaN:Si	3000 nm

TABLE II
PARAMETERS EXTRACTED FROM MEASUREMENTS IN FIG. 2

Name	Value
QW SRH lifetime	20 ns
QW Auger coefficient	4.3 10 ⁻³⁰ cm ⁶ /s
free-carrier absorption cross section	6 10 ⁻¹⁷ cm ²
p-cladding acceptor density	10 ²⁰ cm ⁻³
p-cladding hole mobility	2 cm ² /Vs
residual series resistance	0.35 Ω

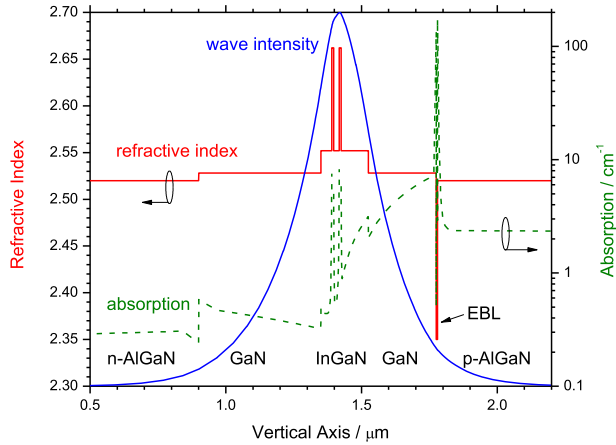


Fig. 1. Vertical profiles of the refractive index [5], absorption (dashed), and lasing mode intensity (normalized) as calculated at I=4A (EBL – p-AlGaIn electron blocker layer).

recombination with a temperature-independent coefficient $C = 4.3 \cdot 10^{-30} \text{ cm}^6/\text{s}$, which lies within the range of measured numbers [12]. Defect-related SRH recombination has a negligible impact despite the relatively short SRH lifetime of 20 ns assumed inside the QWs. The slope of $P(I)$ is mainly limited by free-carrier absorption [5]. We here adopt a first-principle model for phonon-assisted free-carrier absorption which results in an absorption cross section of $6 \cdot 10^{-17} \text{ cm}^2$ for our case [13]. Without any parameter fitting, this absorption model gives a surprisingly good agreement with the measured $P(I)$ characteristic in Fig. 2. The absorption profile calculated at I=4A is shown in Fig. 1 as dashed line (see below for discussion).

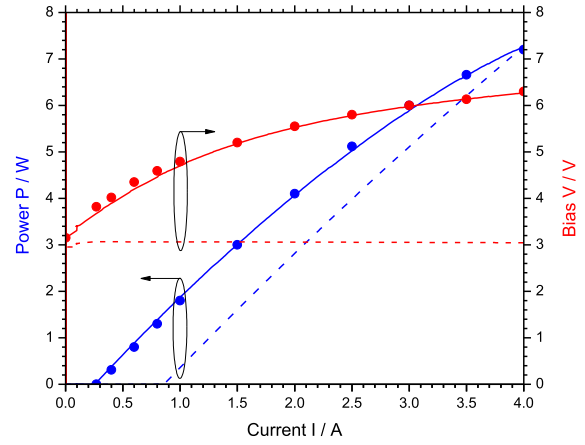


Fig. 2. Comparison between measurements (dots) [5] and CW simulations (solid lines) at T=300K stage temperature. The dashed bias line illustrates the photon energy. The dashed power line shows the calculated output power without self-heating at T=422K.

The calculated internal temperature rise is $\Delta T=122\text{K}$ at I=4A based on the measured thermal resistance of $\Delta T/(IV-P) = 6.6 \text{ K/W}$ [11]. This temperature rise nearly quadruples the density of free holes in the p-AlGaIn cladding layer, due to the large Mg acceptor ionization energy of about 180meV [14]. At room temperature, we calibrate the unknown Mg acceptor density to match the reported hole density of 10^{18} cm^{-3} [5]. The p-AlGaIn hole mobility ($2 \text{ cm}^2/\text{Vs}$) and the residual series resistance ($R_{\text{res}} = 0.35\Omega$) are then adjusted to achieve agreement with the bias measurement in Fig. 2. The large ionization energy of Mg acceptors requires a high Mg density that reduces the hole mobility by scattering. The residual resistance accounts for all contributions outside the simulated region, in particular for the contact resistance. Our result R_{res} translates into the specific resistivity of $0.05 \text{ m}\Omega/\text{cm}^2$ which is slightly lower than a reported p-GaN contact resistivity of $0.1 \text{ m}\Omega/\text{cm}^2$ [15]. Due to limited data [5], a possible temperature dependence of the p-contact resistance cannot be separated from that of the p-cladding. However, the sub-linearity of the measured bias-current characteristic can be explained by thermal activation of holes in the p-AlGaIn cladding layer. But the excess bias above the photon voltage of $h\nu/q = 3.05\text{V}$ is still 3.2V at I=4A (Fig. 2). Residual resistance and p-AlGaIn cladding layer contribute almost equally to this excess bias, about 1.4V each. The remaining 0.4V are mainly caused by hetero-interfaces. At lower current, the p-cladding clearly dominates the series resistance.

Encouraged by the good agreement between simulation and measurement, we now examine the impact of internal processes on the wall-plug efficiency. Most importantly, the QW material gain is reduced at higher temperature due to the wider spreading of the Fermi distribution of electrons and holes (Fig. 3). Consequently, the QW carrier density $n_{\text{th}}(I)$ rises to maintain the required threshold gain. This translates into a strongly increasing threshold current $I_{\text{th}}(I)$ since the Auger recombination rate rises with the third power of the carrier density (Fig. 4). Such increase is often neglected [6]. The threshold current plot in Fig. 4 sums up all QW recombination processes that do not contribute to stimulated

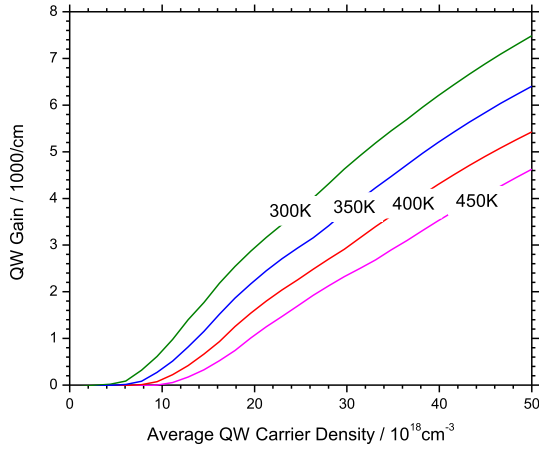


Fig. 3. Quantum well (QW) gain as function of average QW carrier density for different QW temperatures.

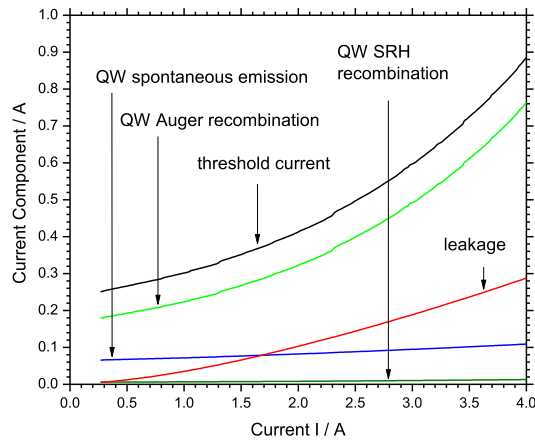


Fig. 4. Components of the total current I consumed by different carrier loss mechanisms.

emission of photons, i.e., Auger recombination, spontaneous emission, and SRH recombination ($I_{th} = I_{Aug} + I_{spont} + I_{SRH}$). Current leakage is caused by electrons escaping from the QWs into the p-side waveguide layers, where they recombine with holes. The leakage current in Fig. 4 is calculated by integration over all recombination processes outside the active layers. The leakage contribution to the initial room-temperature threshold current is negligible in our case and we do not include it in the calculation of the threshold current. Instead, the leakage current I_{leak} is fully accounted for by $\eta_i = I_{stim}/(I - I_{th}) = I_{stim}/(I_{stim} + I_{leak})$ with I_{stim} feeding stimulated recombination ($I = I_{th} + I_{leak} + I_{stim}$). This way, the effects of leakage and Auger recombination are clearly separated in our efficiency analysis below. For confirmation, we perform a simulation without self-heating at $T=422K$ stage temperature which results in a threshold current of 860mA (dashed power line in Fig. 2) that is very close to the threshold current given in Fig. 4 at $I=4A$ and $T_{QW} = 422K$. Using $I_{th} \propto \exp(T/T_0)$, we obtain the characteristic temperature $T_0 = 96K$ which is within the range 90K-230K observed at similar emission wavelengths [16]. Measured T_0 values are not reported for our reference laser.

Electron leakage from the QWs leads to carrier accumulation in the p-side waveguide layers which causes 65% of the total absorption of $\alpha_i = 2/cm$ at $I=4A$. Strong hole

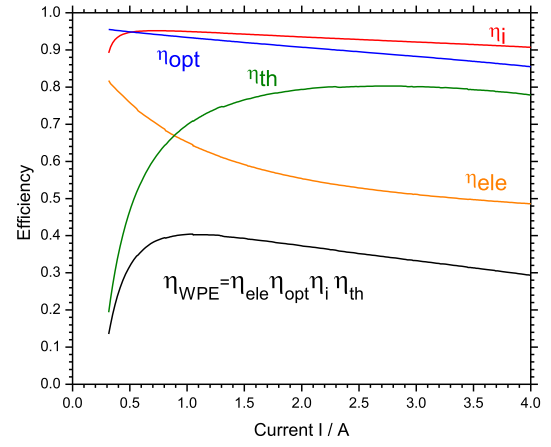


Fig. 5. Efficiencies vs. current (η_{WPE} - wall-plug efficiency, η_{ele} - electrical efficiency, η_{opt} - optical efficiency accounting for front and back emission from the laser diode, η_i - differential internal efficiency, η_{th} - threshold current efficiency).

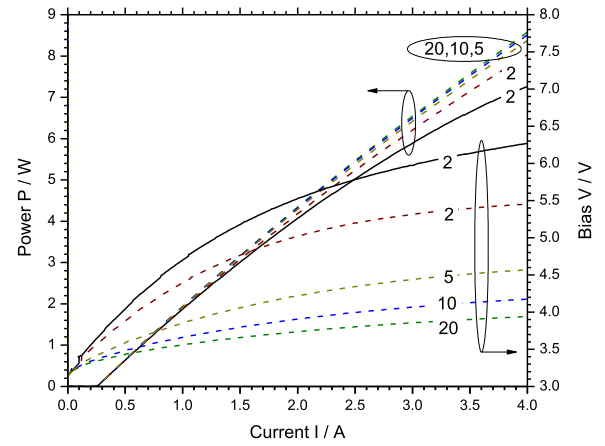


Fig. 6. Power and bias vs. current with the p-AlGaIn cladding layer hole mobility as parameter (in cm^2/Vs). The solid lines are from the original simulation with $R_{res} = 0.35\Omega$ residual resistance. The dashed lines are for $R_{res} = 0$.

accumulation at the EBL accounts for about 20% and the thermally activated holes inside the p-AlGaIn cladding layer contribute only 2% to the optical loss due to the small overlap with the laser mode (see Fig. 1).

Figure 5 plots the main results of this paper, namely the different components of the wall-plug efficiency. Current leakage (η_i) has the smallest influence at high power, followed by internal absorption (η_{opt}) and Auger recombination (η_{th}); however, leakage is mainly responsible for the rising absorption. The most serious efficiency limitation originates in the decline of the electrical efficiency η_{ele} with increasing current, due to the rising bias. This is attributed to the large series resistance that is partially rooted in the low hole mobility inside the p-AlGaIn cladding layer. Therefore, alternative solutions are currently explored, such as tunnel-junctions [15], or indium-tin-oxide cladding layers [17].

The influence of the series resistance is further studied by varying key parameters in the simulation (see Figs. 6 and 7). Elimination of the residual resistance lowers the bias at 4A by 1.4V but raises the peak wall-plug efficiency only slightly to 44%. An additional elevation of the p-AlGaIn hole mobility

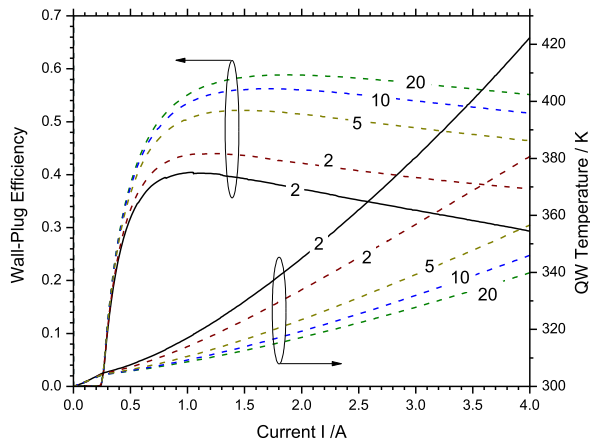


Fig. 7. Wall-plug efficiency and quantum well (QW) temperature vs. current with the p-AlGaIn cladding layer hole mobility as parameter (in cm^2/Vs). The solid lines are from the original simulation with $R_{\text{res}} = 0.35\Omega$ residual resistance. The dashed lines are for $R_{\text{res}} = 0$.

to $20 \text{ cm}^2/\text{Vs}$ results in more than 55% wall-plug efficiency at $I=4\text{A}$, mainly based on the reduced bias of 3.9V and the improved electrical efficiency of 77%. The lower series resistance also lowers the self-heating which limits the rise of threshold density $n_{\text{th}}(I)$ and threshold current $I_{\text{th}}(I)$ so that the output power is enhanced. Even a modest mobility enlargement to $5 \text{ cm}^2/\text{Vs}$ already yields significant performance improvements in Figs. 6 and 7.

In summary, we identified the high series resistance as main reason for the low power conversion efficiency of high-power GaN-based lasers. We also propose an improved analysis of sub-linear power-current characteristics by considering the rise of the threshold current and by clearly separating the influence of different loss mechanisms.

REFERENCES

- [1] S. Nakamura, "Background story of the invention of efficient blue InGaIn light emitting diodes," *Rev. Mod. Phys.*, vol. 87, p. 1139, Oct. 2015.
- [2] C. A. Humi *et al.*, "Bulk GaN flip-chip violet light-emitting diodes with optimized efficiency for high-power operation," *Appl. Phys. Lett.*, vol. 106, no. 3, p. s031101, 2015.
- [3] J. W. Raring, "Laser diodes for next generation light sources," in *Proc. DOE SSL R&D Workshop*, Raleigh, NC, USA, 2016, pp. 1–13.

- [4] A. Loeffler *et al.*, "InGaIn power laser chips in a novel 50W multi-die package," *Proc. SPIE*, vol. 9363, p. 936318, Mar. 2015.
- [5] M. Kawaguchi *et al.*, "Optical-loss suppressed InGaIn laser diodes using undoped thick waveguide structure," *Proc. SPIE*, vol. 9748, p. 974818, Feb. 2016.
- [6] P. Crump *et al.*, "Efficient high-power laser diodes," *IEEE J. Sel. Topics Quantum Electron.*, vol. 19, no. 14, p. 1501211, Jul./Aug. 2013.
- [7] J. J. Wierer, Jr., J. Y. Tsao, and D. S. Sizov, "Comparison between blue lasers and light-emitting diodes for future solid-state lighting," *Laser Photon. Rev.*, vol. 7, no. 6, pp. 963–993, 2013.
- [8] LASTIP by Crosslight Software Inc., Vancouver, BC, Canada, 2016.
- [9] J. Piprek and S. Nakamura, "Physics of high-power InGaIn/GaN lasers," *IEE Proc.-Optoelectron.*, vol. 149, no. 4, pp. 145–151, Aug. 2002.
- [10] J. Piprek, *Semiconductor Optoelectronic Devices: Introduction to Physics and Simulation*, San Diego, CA, USA: Academic, 2003.
- [11] S. Nozaki *et al.*, "High-power and high-temperature operation of an InGaIn laser over 3 W at 85 °C using a novel double-heat-flow packaging technology," *Jpn. J. Appl. Phys.*, vol. 55, no. 4S, p. 04EH05, 2016.
- [12] J. Piprek, F. Roemer, and B. Witzigmann, "On the uncertainty of the Auger recombination coefficient extracted from InGaIn/GaN light-emitting diode efficiency droop measurements," *Appl. Phys. Lett.*, vol. 106, no. 10, p. 101101, 2015.
- [13] E. Kioupakis, P. Rinke, and C. G. Van de Walle, "Determination of Internal Loss in Nitride Lasers from First Principles," *Appl. Phys. Exp.*, vol. 3, no. 8, p. 082101, 2010.
- [14] J. Piprek, "How to decide between competing efficiency droop models for GaIn-based light-emitting diodes," *Appl. Phys. Lett.*, vol. 107, no. 3, p. 031101, 2015.
- [15] B. P. Yonkee *et al.*, "Demonstration of a III-nitride edge-emitting laser diode utilizing a GaIn tunnel junction contact," *Opt. Exp.*, vol. 24, no. 25, p. 256556, 2016.
- [16] A. Bojarska *et al.*, "Emission wavelength dependence of characteristic temperature of InGaIn laser diodes," *Appl. Phys. Lett.*, vol. 103, no. 7, p. 071102, 2013.
- [17] A. Pourhashemi, R. M. Farrell, D. A. Cohen, J. S. Speck, S. P. DenBaars, and S. Nakamura, "High-power blue laser diodes with indium tin oxide cladding on semipolar (2021) GaIn substrates," *Appl. Phys. Lett.*, vol. 106, no. 11, p. 111105, 2015.

Joachim Piprek received the Diploma and Ph.D. degrees in physics from Humboldt University, Berlin, Germany. For more than two decades, he worked in industry and academia on design, simulation, and analysis of various semiconductor devices used in optoelectronics. He is currently the President of the NUSOD Institute. Dr. Piprek has authored three books, six book chapters, and about 250 papers with over 6000 citations. He is the Founder and a Co-Chair of the annual conference on Numerical Simulation of Optoelectronic Devices (IEEE) and he also chaired several SPIE conferences. Dr. Piprek was an invited Guest Editor for various special journal issues on optoelectronic device simulation. He currently serves as the Editor of the two-volume *Handbook of Optoelectronic Device Modeling and Simulation* (Taylor & Francis, 2017) and as an Executive/Associate Editor for two research journals.